THE JOURNAL OF PHYSICAL CHEMISTRY B

Article

Cite This: J. Phys. Chem. B 2019, 123, 9719−9723

pubs.acs.org/JPCB

Hydrogen Bond Preserving Stress Release Mechanism Is Key to the Resilience of Aramid Fibers

Subodh C. Tiwari,[†] Kohei Shimamura,[‡] Ankit Mishra,[†] Fuyuki Shimojo,[§] Aiichiro Nakano,[†] Rajiv K. Kalia,[†] Priya Vashishta,[†] and Paulo S. Branicio*[,†]

[†]Collaboratory for Advanced Computing and Simulations, Department of Physics & Astronomy, Department of Computer Science, Department of Chemical Engineering & Materials Science, and Department of Biological Sciences, University of Southern California, Los Angeles, California 90089-0242, United States

[‡]Graduate School of System Informatics, Kobe University, Kobe 657-8501, Japan

[§]Department of Physics, Kumamoto University, Kumamoto 860-8555, Japan

Supporting Information

ABSTRACT: *Ab initio* molecular dynamics simulations of shock loading on poly(*p*-phenylene terephthalamide) (PPTA) reveal stress release mechanisms based on hydrogen bond preserving structural phase transformation (SPT) and planar amorphization. The SPT is triggered by [100] shock-induced coplanarity of phenylene groups and rearrangement of sheet stacking leading to a novel monoclinic phase. Planar amorphization is generated by [010] shock-induced scission of hydrogen bonds leading to disruption of polymer sheets, and *trans*-to-*cis* conformational change of polymer chains. In contrast to the latter, the former mechanism preserves the hydrogen bonding and cohesiveness of polymer chains in the identified novel crystalline phase preserving the strength of PPTA. The interplay between hydrogen bond preserving (SPT) and nonpreserving (planar amorphization) shock release mechanisms is critical to understanding the shock performance of aramid fibers.

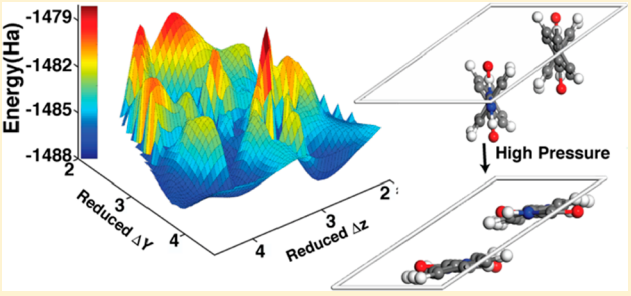

INTRODUCTION

Aramid fibers, such as Kevlar and Twaron, are of great interest due to their outstanding ratio of strength per weight and thermal resistance.[1,2] There are numerous applications of these fibers that include bulletproof vests and helmets, turbine engine fragment, containment structures, cut resistant gloves, etc.[3−6] Compositional and structural studies of aramid fibers suggest that these materials derive their exceptional properties from crystalline domains of poly(*p*-phenylene terephthalamide) (PPTA) polymers, highly oriented along the fiber axis.[7−11] Figure 1a illustrates the aramid fiber structure. While aramid fibers display exceptional performance, their development and improvement have been historically empirical and based on trial and error.[12,13] Recent investigations on the effect of defects on the performance of fibers have been instrumental in understanding intrinsic deformations and failure mechanisms.[14−16] However, there is a startling lack of shock investigations on PPTA and aramid fibers.[17,18] Since the main application of these fibers is in shock and impact protection, such studies are required for understanding the intrinsic stress release mechanisms of PPTA.

Atomistic simulations are key to understanding shock damage microscopically and to enable atomistically informed continuum simulations.[19−21] Recent simulations have highlighted the influence of defects, and the arrangement of chain structures, on the mechanical properties.[14−16,22,23] Nevertheless, in order to understand the intrinsic ability of aramid fabrics to withstand shock loading, the response of its most basic constituent, PPTA crystals, needs to be investigated explicitly first. The shock response of the intricate bond-hierarchy-stabilized PPTA structure can be modeled accurately by first-principles methods.[24,25]

METHODS

In this work, we investigate the shock response of PPTA using the multiscale shock technique (MSST) with the PBE functional and empirical DFT-D to incorporate van der Waals interactions.[26−28] The MSST equations of motion are integrated numerically with a time step of 10 au (~0.242 fs) for up to 5 ps. MSST simulations are performed perpendicular to PPTA chains along the [100] and [010] crystallographic directions, at several particle velocities in the range 0.24−4 km/s. This range of particle velocities probes the different expected response regimes of the PPTA crystal to shock loading, i.e., from very weak shock (elastic response) to strong shock (cross-linking response). The PPTA crystal structure is

Received: August 27, 2019
Revised: October 17, 2019
Published: October 23, 2019

DOI: 10.1021/acs.jpcb.9b08168
J. Phys. Chem. B 2019, 123, 9719−9723

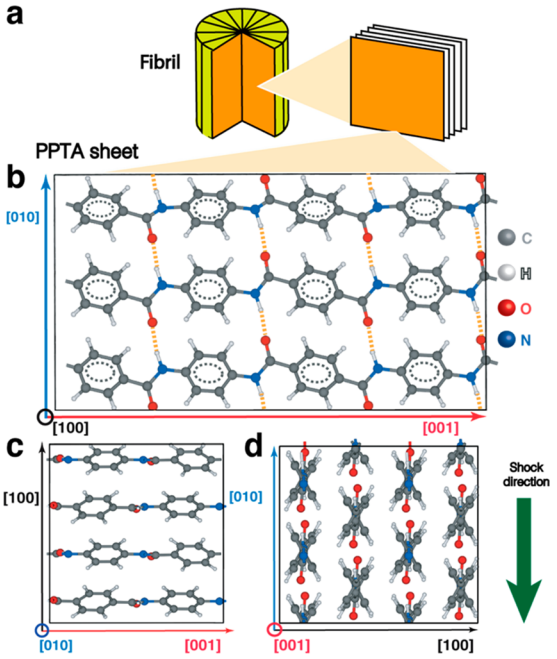

Figure 1. (a) Schematics of an aramid fiber microstructure, composed of elongated, highly crystalline fibrils where PPTA polymer chains are aligned along the fibril length forming stacked PPTA sheets. (b) Structure of PPTA sheet with in-plane hydrogen bonding indicated by orange dotted lines. (c) PPTA crystal oriented along [010], highlighting the PPTA sheet stacking structure. (d) PPTA crystal oriented along the polymer chain, [001] (fibril length). Gray, white, red, and blue spheres correspond to carbon, hydrogen, oxygen, and nitrogen atoms, respectively.

highly anisotropic along the low index crystallographic directions [100], [010], and [001]. Covalent bonding between monomers forms long polymer chains along the [001] direction (shown in Figure 1b). In-plane hydrogen bonding along the [010] direction forms polymer sheets (hydrogen bonding is indicated by the dotted lines in Figure 1b). In the [100] direction, PPTA sheets are stacked in ABAB arrangement and interact by weaker van der Waals interactions (shown in Figure 1c,d). Therefore, distinct types of bonding exist in each direction of the crystal, i.e., covalent along the chain axis, hydrogen bonds within sheets, and van der Waals between different sheets. This bond hierarchy leads to highly anisotropic mechanical properties; i.e., high tensile strength and modulus along the chain axis contrast with the corresponding compressive properties and with the mechanical properties along other directions. This anisotropy of mechanical properties requires a careful consideration in the design of the fibers.[1,29,30] The manufacturing process of commercial fibers, such as Kevlar and Twaron, take advantage of the PPTA crystal structure by producing highly aligned polymer chains along the fiber axis.

RESULTS AND DISCUSSION

The shock Hugoniot curves of the PPTA crystal along the [100] and [010] directions are presented in Figure 2a,b. Corresponding pressure plots are displayed in the Supporting Information, Figure S2a,b. Discontinuous changes in shock Hugoniot curves correspond to transitions between different shock response regimes. For shock direction [100] we observe discontinuity at U_p = 2.07 km/s and U_p = 2.66 km/s. The former corresponds to a PPTA structural phase transformation (SPT), and the latter corresponds to cross-linking of the polymer chains. Along [010], a first discontinuity at U_p = 0.4 km/s indicates a transition from the elastic regime to the plastic regime and the second discontinuity at U_p = 3.24 km/s is related to polymer chain cross-linking.

For weak shocks, the PPTA crystal response shows a highly anisotropic elastic compression regime along different directions. For shock along [100], we observe high volume reduction leading to compaction of the polymer sheets and conformational changes in the PPTA polymer chains. The volume is reduced up to 29% at 2.07 km/s. The distance between PPTA sheets is reduced from 4.6 to3.9 Å. For elastic shock along [010], we observe a relatively low volume reduction up to 6% at 0.4 km/s before plasticity is triggered. In unshocked PPTA, the two phenylene groups are arranged at opposite dihedral angle with the amide group as shown in Figure 1b (label for dihedral is given in Figure S3). The dihedral angle for unshocked PPTA is 26°. In the elastic regime, the dihedral angle evolution as a function of time is shown in Figure 2i for shock along both [100] (in blue) and [010] (in red) directions. In the case of the [100] direction, the dihedral angle reduces from 26 to 16° at 2.07 km/s. In contrast, the dihedral angle along [010] remains unchanged. Animation movies for the elastic process are in the Supporting Information (movie S1 for the [100] direction and movie S2 for the [010] direction).

For strong shocks, we observe cross-linking of the PPTA polymer chains with the formation of new bonds between chains, which drastically changes its chemical structure. A similar phenomenon was reported for ethane clusters under impact resulting in polymerization.[31] We have quantified this process by monitoring the integrity of the PPTA backbone, where all carbon atoms have sp^2 hybridization. Figure 2k shows the fraction of sp^2 carbon present in the system as a function of time in both cases. For the [100] direction, we observe a drastic drop in the fraction of sp^2 carbon at U_p = 3.42 km/s. A similar behavior is observed for the [010] direction at U_p = 3.7 km/s. Animation movies for the cross-linking process are provided in the Supporting Information (movie S3 for the [100] direction, movie S4 for the [010] direction).

PPTA displays an intriguing shock response in the intermediate shock regime of 1.44 < U_p < 3.24 km/s along [010]. We observe a plastic response characterized by (i) a massive scission of hydrogen bonds, (ii) rotation of whole polymer chains, (iii) independent rotation of phenylene and amide groups, (iv) change in the conformation from *trans*-to-*cis* (movie S5), and (v) misalignment of polymer chains. All these mechanisms are illustrated by movie S6. The *trans*-to-*cis* conformational change, shown in Figure 3a,b, has a particular deleterious effect on the PPTA crystal, which distorts and stresses the polymer backbone, affecting its ability to regenerate hydrogen bonding with neighboring molecules in the sheets. This shock release mechanism is akin to the shock induced *trans*-to-*gauche* isomerization reported for self-assembled hydrocarbon monolayers.[32] All the listed plastic mechanisms act to destabilize the polymer sheets as shown in Figure 2g. Figure 2j shows up to an 80% drop in the number of hydrogen bonds. This plastic response effectively destroys the long-range order of the crystalline alignment of the polymer chains leading to a planar amorphous phase, where polymer chains are weakly bonded by van der Waals interactions and contain both *trans* and *cis* conformations. The disordered

DOI: 10.1021/acs.jpcb.9b08168
J. Phys. Chem. B 2019, 123, 9719−9723

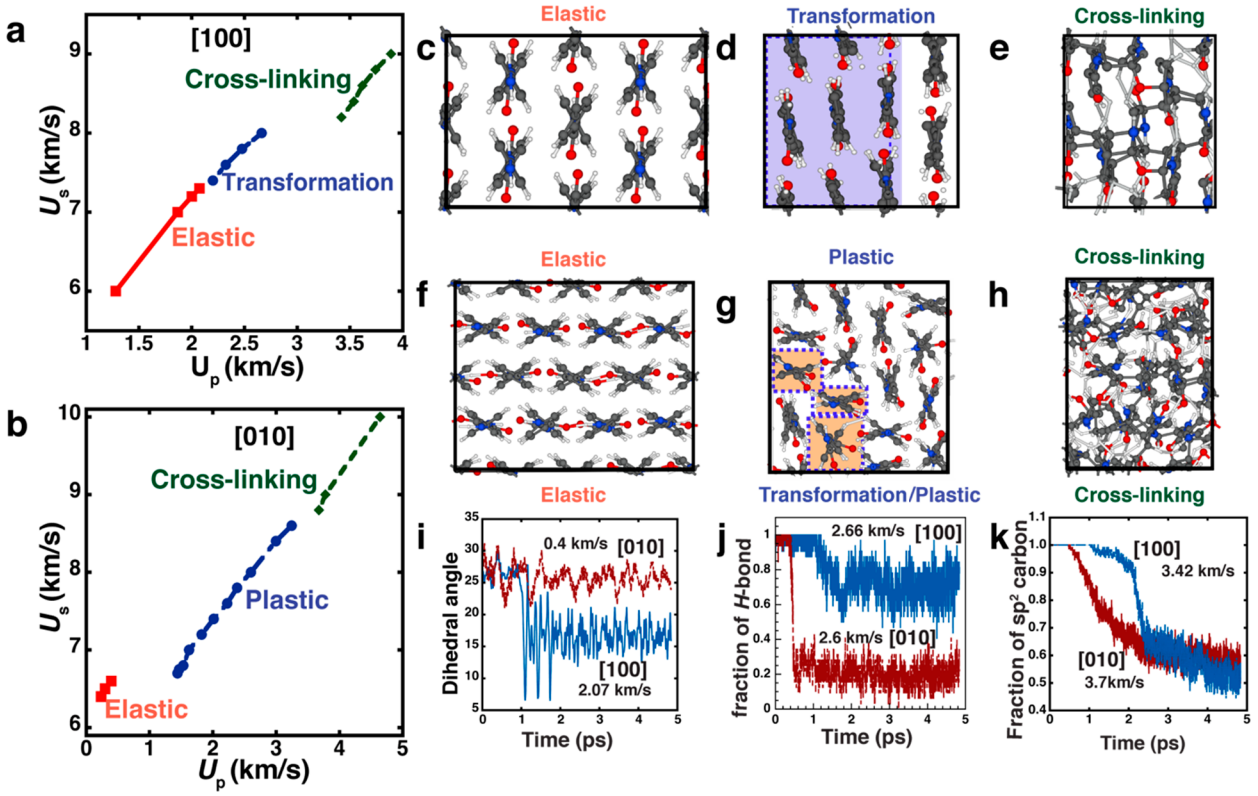

Figure 2. Shock Hugoniot curves along [100] (a) and [010] directions (b), respectively. PPTA structure in elastic (c), transformation (d), and cross-linking (e) regimes for shocks along [100] direction and (f–h) along [010] direction, respectively. Chains undergoing structural or *trans*–*cis* transformation are highlighted. (i–k) Analysis of structural changes in different regimes by the evolution of dihedral angle between phenylene and amide groups in the elastic regime, fraction of hydrogen bonds preserved in the plastic/transformation regimes, and fraction of sp^2 preserved in the cross-linking regime.

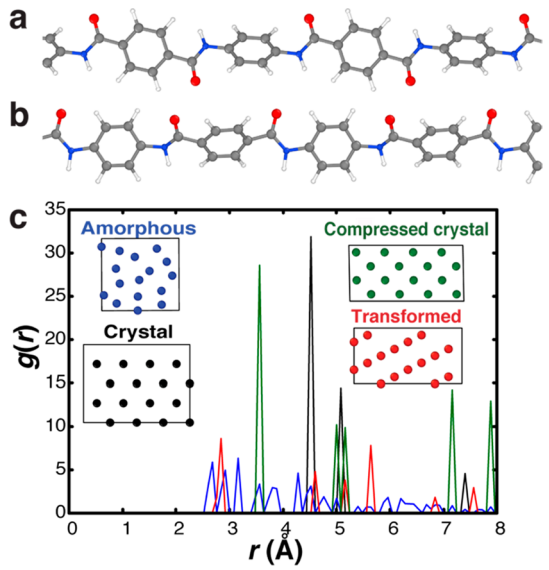

Figure 3. *trans* (a) and *cis* (b) conformations of a PPTA polymer chain. PPTA crystals have 100% *trans* conformation; 20% of polymer chains transform to *cis* during shock along the [010] direction, leading to a planar amorphous phase. (c) Radial distribution function of polymer chain center of mass in the (001) plane for crystalline (C), planar amorphous (A), compressed crystalline (c-C), and transformed (T) systems. The insets show the corresponding center-of-mass configurations.

arrangement of the polymer chains is quantified by the radial distribution function, $g(r)$, of their center-of-mass positions shown in Figure 3c. Sharp peaks in $g(r)$ are lost in the planar amorphous phase, indicating lack of crystalline arrangement.

In sharp contrast to the shock response along [010], the intermediate shock regime along [100], between U_p = 2.07 km/s and U_p = 2.66 km/s, leads to a pressure-induced SPT that preserves the integrity of the PPTA polymer sheets and the *trans* conformation of the polymer chains. SPT is a common shock release mechanism in strongly bonded materials.[33] The evolution of PPTA during the SPT is illustrated in movie S7. Results indicate that for some polymer chains the phenylene group attached to the carbonyl end of the amide group reverses its orientation with respect to the amide group, making both phenylene groups coplanar. This conformational change induces displacement of polymer sheets in both [010] and [001] directions and the stacking rearrangement propagates to neighboring polymer sheets as illustrated in the movie S7. Since these simulations are computationally costly, the shock response is simulated up to 4.88 ps. During this short time period the identified transformation is incomplete for the particle velocities considered here. Please see Figure 2d for a partially transformed system at U_p = 2.2 km/s.

To uniquely identify the structure of the transformed phase, we perform global energy minimization by sampling the phase space using the Bayesian optimization method. Bayesian optimization method pseudocode is provided in Table S1, and the result is shown in Figure S4. The dimensionality reduction and Bayesian optimization process is described in

DOI: 10.1021/acs.jpcb.9b08168
J. Phys. Chem. B 2019, 123, 9719–9723

detail in Supporting Information. We evaluate the energy landscape of PPTA in the compressed state as a function of individual polymer chains displacement in the [010] and [001] directions. The calculated energy landscape is shown in Figure 4a. Energy values are plotted as a function of reduced

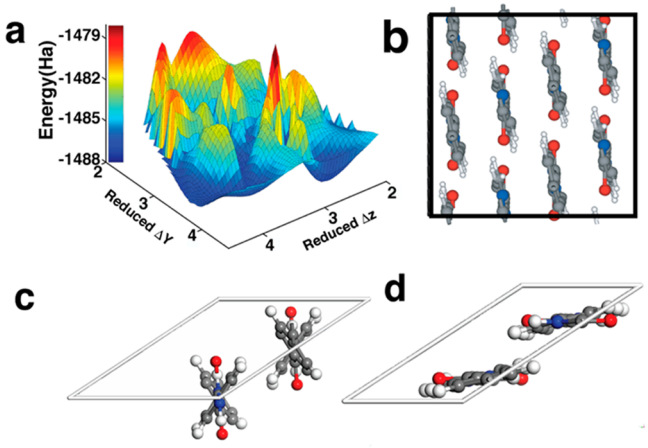

Figure 4. (a) Energy landscape of the compressed system as a function of polymer chains' reduced displacement in [010] and [001] directions. Reduced displacements are calculated using Gödel encoding (see the Supporting Information). (b) Predicted new phase of PPTA under shock along the [100] direction. All the phenylene groups in polymer chains are coplanar in this PPTA phase. (c) Unshocked PPTA monoclinic primitive unit cell. (d) Predicted new phase PPTA monoclinic primitive unit cell.

displacements, Δy and Δz, corresponding to the [010] and [001] directions, calculated using Gödel encoding (see the Supporting Information). The predicted structure is further verified by the meta-GGA method (see the Supporting Information, Figure S5). The predicted structure displays the previously described rotation of one phenylene group. The phenylene group attached to the carbonyl (oxygen) end of an amide flip its orientation and becomes coplanar to the phenylene group attached to the amine (nitrogen) end of an amide (geometry shown in Figure 4b). Symmetry analysis of the predicted structure indicates that it belongs to the same monoclinic space group as the original PPTA crystal $P2_1/c$. Figure 4 shows the primitive cells of the original and transformed systems. The primitive cell of the transformed system shows 90° rotation of the hydrogen bonded PPTA sheets and coplanarity of the phenylene groups. Given the similarity in space group, the $g(r)$ of the transformed structure, shown in Figure 3c, contrasts with the $g(r)$ of the crystalline structure. We observe a new peak at 2.8 Å indicating the highly compact stacking.

The predicted anisotropic shock response of PPTA along the independent directions perpendicular to the polymer chain axis offers a framework to understand the outstanding behavior of aramid fibers and its failure mechanism. Our results show that the SPT induced by shock in [100] preserves the in-plane hydrogen bonding which is linked to the observed strength of PPTA. In contrast, the complete breakdown of hydrogen bonding for shock in [010] shifts the failure mechanism from chain rupture to chain pullout, as identified in polyethylene fibers.[14] This process is expected to significantly reduce the tensile strength of PPTA. The effect of hydrogen bonding in the PPTA crystal is similar to β-sheet crystal domains in silk.[34]

Considering our results, each randomly oriented fibril may present a widely different shock response; i.e., a [100] oriented fibril will outperform [010] oriented fibril under compressive shock. The latter arguably will lose its strength in the plastic regime which starts at modest particle velocities of $U_p \sim 0.4$ km/s. This loss of strength linked to hydrogen bond disruption may explain the fibrillation failure process identified as a major failure mode in Kevlar fibers.[15] Fibrillation of aramid fibers under impact is a predominant failure mechanism that is not well understood.

CONCLUSION

In conclusion, we used *ab initio* molecular dynamics of shock loading based on the multiscale shock technique to describe the response of PPTA crystals to shock loading of different intensities. The results revealed a highly anisotropic shock response involving a hydrogen bond preserving structural phase transformation, for shock along [100], and planar amorphization, for shock along the [010] direction. These two distinct shock release mechanisms may help in the understanding of the outstanding performance displayed by aramid fibers and their failure mechanisms, which involve a fibrillation failure process. Our results suggest that the strengthening of aramid polymers produced by the drawing process, which results in highly aligned crystalline domains along the fiber axis, could be significantly enhanced if the superior shock performance of the PPTA [100] direction could be further explored in novel fiber processing and fabric design.

ASSOCIATED CONTENT

Supporting Information

The Supporting Information is available free of charge on the ACS Publications website at DOI: 10.1021/acs.jpcb.9b08168.

Simulation details, omnidirectional multiscale shock technique implementation, details on Bayesian optimization (PDF)
Elastic shock from [100] direction (MOV)
Elastic shock from [010] direction (MOV)
Cross-linking shock from [100] direction (MOV)
Cross-linking shock from [010] direction (MOV)
Transformation shock from [100] direction (MOV)
Plastic shock from [010] direction (MOV)
cis−*trans* transformation during shock from [010] direction (MOV)

AUTHOR INFORMATION

Corresponding Author

*E-mail: branicio@usc.edu.

ORCID

Subodh C. Tiwari: 0000-0002-5516-6900
Kohei Shimamura: 0000-0003-3235-2599
Aiichiro Nakano: 0000-0003-3228-3896
Priya Vashishta: 0000-0003-4683-429X
Paulo S. Branicio: 0000-0002-8676-3644

Notes

The authors declare no competing financial interest.

ACKNOWLEDGMENTS

The work was supported by Grant DE-SC0018195 funded by the U.S. Department of Energy, Office of Science. Simulations were performed at the Argonne Leadership Computing Facility

DOI: 10.1021/acs.jpcb.9b08168
J. Phys. Chem. B 2019, 123, 9719−9723

under the DOE INCITE program and at the Center for High Performance Computing of the University of Southern California. We would like to acknowledge USC-HPC for providing computing resources.

REFERENCES

(1) Northolt, M. G.; Den Decker, P.; Picken, S. J.; Baltussen, J. J. M.; Schlatmann, R. The Tensile Strength of Polymer Fibres. In *Polymeric and Inorganic Fibers*; Springer-Verlag: Berlin, 2005; Vol. *178*, pp 1−108.
(2) Chatzi, E. G.; Koenig, J. L. Morphology and Structure of Kevlar Fibers: A Review. *Polym.-Plast. Technol. Eng.* **1987**, *26*, 229−270.
(3) Guoqi, Z.; Goldsmith, W.; Dharan, C. H. K. H. Penetration of Laminated Kevlar by Projectiles-I. Experimental Investigation. *Int. J. Solids Struct.* **1992**, *29*, 399−420.
(4) Mayo, J. B.; Wetzel, E. D. Cut Resistance and Failure of High-Performance Single Fibers. *Text. Res. J.* **2014**, *84*, 1233−1246.
(5) Coleman, W. H.; Chen, D.; Li, Y. Q.; Cowan, A. E.; Setlow, P. How Moist Heat Kills Spores of Bacillus Subtilis. *J. Bacteriol.* **2007**, *189*, 8458−8466.
(6) Peterson, C. W. High-Performance Parachutes. *Sci. Am.* **1990**, *262*, 108−117.
(7) Northolt, M. G. X-Ray Diffraction Study of Poly(p-Phenylene Terephthalamide) Fibres. *Eur. Polym. J.* **1974**, *10*, 799−804.
(8) Dobb, M. G.; Hindeleh, A. M.; Johnson, D. J.; Saville, B. P. Lattice Resolution in an Electron-Beam Sensitive Polymer. *Nature* **1975**, *253*, 189−190.
(9) Young, R. J.; Lu, D.; Day, R. J.; Knoff, W. F.; Davis, H. A. Relationship between Structure and Mechanical Properties for Aramid Fibres. *J. Mater. Sci.* **1992**, *27*, 5431−5440.
(10) Liu, J.; Geil, P. H. Crystal Structure and Morphology of Poly(Ethylene Terephthalate) Single Crystals Prepared by Melt Polymerization. *J. Macromol. Sci., Part B: Phys.* **1997**, *36*, 61−85.
(11) Rao, Y.; Waddon, A. J.; Farris, R. J. Structure-Property Relation in Poly(p-Phenylene Terephthalamide) (PPTA) Fibers. *Polymer* **2001**, *42*, 5937−5946.
(12) Lee, K.-G.; Barton, R.; Schultz, J. M. Structure and Property Development in Poly(p-Phenylene Terephthalamide) during Heat Treatment under Tension. *J. Polym. Sci., Part B: Polym. Phys.* **1995**, *33*, 1−14.
(13) Ahmed, D.; Hongpeng, Z.; Haijuan, K.; Jing, L.; Yu, M.; Muhuo, Y. Microstructural Developments of Poly (p-Phenylene Terephthalamide) Fibers During Heat Treatment Process : A Review. *Mater. Res.* **2014**, *17*, 1180−1200.
(14) O'Connor, T. C.; Robbins, M. O. Chain Ends and the Ultimate Strength of Polyethylene Fibers. *ACS Macro Lett.* **2016**, *5*, 263−267.
(15) Chowdhury, S.; Sockalingam, S.; Gillespie, J. Molecular Dynamics Modeling of the Effect of Axial and Transverse Compression on the Residual Tensile Properties of Ballistic Fiber. *Fibers* **2017**, *5*, 7.
(16) Mercer, B. S. *Molecular Dynamics Modeling of PPTA Crystals in Aramid Fibers*. Ph.D. Dissertation, University of California, Berkeley, 2016.
(17) Homae, T.; Shimizu, T.; Fukasawa, K.; Masamura, O. Hypervelocity Planar Plate Impact Experiments of Aramid Fiber-Reinforced Plastics. *J. Reinf. Plast. Compos.* **2006**, *25*, 1215−1221.
(18) Shim, V. P. W. P. W.; Lim, C. T. T.; Foo, K. J. J. Dynamic Mechanical Properties of Fabric Armour. *Int. J. Impact Eng.* **2001**, *25*, 1−15.
(19) Sockalingam, S.; Chowdhury, S. C.; Gillespie, J. W.; Keefe, M. Recent Advances in Modeling and Experiments of Kevlar Ballistic Fibrils, Fibers, Yarns and Flexible Woven Textile Fabrics − a Review. *Text. Res. J.* **2017**, *87*, 984−1010.
(20) Grujicic, M.; Glomski, P. S.; Pandurangan, B.; Bell, W. C.; Yen, C.-F.; Cheeseman, B. A. Multi-Length Scale Computational Derivation of Kevlar®yarn-Level Material Model. *J. Mater. Sci.* **2011**, *46*, 4787−4802.
(21) Ortiz, V.; Nielsen, S. O.; Discher, D. E.; Klein, M. L.; Lipowsky, R.; Shillcock, J. Dissipative Particle Dynamics Simulations of Polymersomes. *J. Phys. Chem. B* **2005**, *109*, 17708−17714.
(22) Depner, M.; Schurmann, B. L. Computer Simulation of Aromatic Polyesters Including Molecular Dynamics. *Polymer* **1992**, *33*, 398−404.
(23) Li, Y.; Goddard, W. A. Nylon 6 Crystal Structures, Folds, and Lamellae from Theory. *Macromolecules* **2002**, *35*, 8440−8455.
(24) Brauckmann, J. O.; Zolfaghari, P.; Verhoef, R.; Klop, E. A.; de Wijs, G. A.; Kentgens, A. P. M. Structural Studies of Polyaramid Fibers: Solid-State NMR and First-Principles Modeling. *Macromolecules* **2016**, *49*, 5548−5560.
(25) Avanzini, L.; Brambilla, L.; Marano, C.; Milani, A. Strain-Dependent Vibrational Spectra and Elastic Modulus of Poly(p-Phenylene Terephtalamide) from First-Principles Calculations. *Polymer* **2017**, *116*, 133−142.
(26) Reed, E. J.; Fried, L. E.; Joannopoulos, J. D. A Method for Tractable Dynamical Studies of Single and Double Shock Compression. *Phys. Rev. Lett.* **2003**, *90*, 235503.
(27) Grimme, S. Semiempirical GGA-Type Density Functional Constructed with a Long-Range Dispersion Correction. *J. Comput. Chem.* **2006**, *27*, 1787−1799.
(28) Perdew, J. P.; Burke, K.; Ernzerhof, M. Generalized Gradient Approximation Made Simple. *Phys. Rev. Lett.* **1996**, *77*, 3865−3868.
(29) Penn, L.; Larsen, F. Physicochemical Properties of Kevlar 49 Fiber. *J. Appl. Polym. Sci.* **1979**, *23*, 59−73.
(30) Deteresa, S. J.; Allen, S. R.; Farris, R. J.; Porter, R. S. Compressive and Torsional Behaviour of Kevlar 49 Fibre. *J. Mater. Sci.* **1984**, *19*, 57−72.
(31) Qi, L.; Sinnott, S. B. Polymerization via Cluster−Solid Surface Impacts: Molecular Dynamics Simulations. *J. Phys. Chem. B* **1997**, *101*, 6883−6890.
(32) Patterson, J. E.; Lagutchev, A.; Huang, W.; Dlott, D. D. Ultrafast Dynamics of Shock Compression of Molecular Monolayers. *Phys. Rev. Lett.* **2005**, *94*, 015501.
(33) Kadau, K.; Germann, T. C.; Lomdahl, P. S.; Holian, B. L. Microscopic View of Structural Phase Transitions Induced by Shock Waves. *Science* **2002**, *296*, 1681−1684.
(34) Keten, S.; Xu, Z.; Ihle, B.; Buehler, M. J. Nanoconfinement Controls Stiffness, Strength and Mechanical Toughness of Beta-Sheet Crystals in Silk. *Nat. Mater.* **2010**, *9*, 359−367.

DOI: 10.1021/acs.jpcb.9b08168
J. Phys. Chem. B 2019, 123, 9719−9723